Chapter 7
Non-Noble Metal Electrocatalysts for the Oxygen Reduction Reaction in Fuel Cells

I. L. Alonso-Lemus and M. Z. Figueroa-Torres

Abstract Low temperature fuel cells are promising and sustainable alternative in energy generation. However, their large-scale production have been limited due at high-cost and scarce electrocatalysts based commonly in noble metals. Development of non-noble electrocatalysts has become intensive in recent years. A wide variety of materials as perovskite-type, spinel-type oxides, tungsten carbides, and heteroatom-doped carbons has been explored as alternative electrocatalysts to platinum. They have demonstrated promising electrocatalytic activity toward the oxygen reduction reaction (ORR) in alkaline electrolytes. However, these electrocatalysts are not favorable using strong acid electrolytes. Moreover, transition metal macrocycles show activity performance close to those of Pt-based electrocatalysts in acid media. In this chapter, we present the most recent developments regarding non-noble metal electrocatalyst, starting with a review of some basic electrochemistry concepts and some techniques commonly used to evaluate their performance. Then, materials used as non-noble metal electrocatalyst are presented which are divided into two groups: (1) the most promising non-noble metal electrocatalysts used in acid electrolytes and (2) in alkaline media. Finally, the conclusions and futures perspective are mentioned for these materials that should be considered as the future electrocatalysts for sustainable large-scale fuel cell commercialization.

Keywords Oxygen reduction reaction · Metal-free electrocatalysts · Transition metal chalcogenide · Transition metal macrocycles · Transition metal nitride · Transition metal carbide · Perovskites · Spinel oxide · Heteroatom-doped carbon · Biomass · Nitrogen precursor · Heteroatom precursor · Koutecky-Levich · 4 electron pathway · 2 electron pathway · Alkaline media · Acid media · Non-noble metal electrocatalysts · Rotating-ring disk electrode · Rotating disk electrode

I. L. Alonso-Lemus (✉)
CONACyT, Sustentabilidad de los Recursos Naturales y Energía, CINVESTAV Unidad Saltillo, Parque Industrial Saltillo-Ramos Arizpe 25900, Ramos Arizpe, Coahuila, Mexico

M. Z. Figueroa-Torres
Universidad Autónoma de Nuevo León, Facultad de Ingeniería Civil, Ciudad Universitaria. 66455, San Nicolás de los Garza, Nuevo León, Mexico

F. J. Rodríguez-Varela, T. W. Napporn (eds.), *Advanced Electrocatalysts for Low-Temperature Fuel Cells*, https://doi.org/10.1007/978-3-319-99019-4_7

7.1 Introduction

The oxygen reduction reaction (ORR) plays a key role in several important processes such as energy conversion, gas sensors, and biology. In energy conversion systems as fuel cells and metal–air batteries, the ORR takes place in the cathode of the device. This reaction is a complex electrochemical process, that is involving multi-electron transfer, which occurs mainly by two pathways: the direct 4-electron reduction pathway and the 2-electron reduction pathway. Additionally, 1-electron reduction pathway can also occur in nonaqueous aprotic solvents and/or in alkaline solutions.

Moreover, the ORR kinetics is very slow; for this reason, to speed up its kinetics a cathode ORR catalyst is needed. Platinum (Pt)-based catalysts are the most used in low temperature fuel cells. However, it is known that Pt-based catalysts are too expensive for making viable the large-scale commercialization of fuel cells. Extensive research over the past several decades has focused on developing alternative catalysts, including non-noble metal catalysts [1].

In this chapter, the most recent advances in the development of non-noble metal catalysts are reviewed. In the first section, we focus on the ORR background information, including the reaction kinetics and mechanisms in acid and alkaline media of the most studied ORR catalysts: platinum, followed by the conventional techniques for electrochemical measurements. The following sections address the wide variety of non-noble metal catalysts that have been developed in recent years, which were classified into two major groups: non-noble catalysts for proton exchange membrane fuel cells (PEMFCs), including direct methanol fuel cells (DMFCs) and non-noble metal catalysts for anion exchange membrane fuel cells anion exchange fuel cells (AEMFC).

Catalysts for PEMFCs include transition metal macrocyclic compounds, transition metal chalcogenides, metal nitrides, oxynitrides, and carbonitrides. On the other hand, catalysts for AEMFC include perovskite, transition metal oxides with spinel structure, and heteroatom-doped carbon materials. The chemical structure of each group of electrocatalysts and the reaction mechanisms proposed for the ORR are discussed in detail in Sects. 7.3 and 7.4 of this chapter.

Finally, a comparison between the catalysts used in acid and basic medium is elucidated, where we discuss from our perspective, what are the biggest challenges and the major areas of opportunity offered by this line of research in the near future.

7.2 Fundamentals of the ORR

The mechanism by which the ORR is carried out currently is complicated to explain, and this depends mainly on the naturalness of the catalyst, surface structure of electrode and the electrolyte. The reaction mechanisms according to the type of

Table 7.1 ORR in different electrolytes and their thermodynamic potential [2]

Electrolyte	Pathway	Reactions	Thermodynamic electrode potential vs. NHE (V)
Acidic	$4e^-$	$O_2 + 4H^+ + 4e^- \rightarrow 2H_2O$	1.299
	$2e^-$	$O_2 + 2H^+ + 2e^- \rightarrow H_2O_2$	0.70
		$H_2O_2 + 2H^+ + 2e^- \rightarrow 2H_2O$	1.76
Alkaline	$4e^-$	$O_2 + 2H_2O + 4e^- \rightarrow 4HO^-$	0.401
	$2e^-$	$O_2 + H_2O + 2e^- \rightarrow HO^- + HO_2^-$	−0.065
		$HO_2^- + H_2O + 2e^- \rightarrow 3HO^-$	0.867
Nonaqueous aprotic solvents	$1e^-$	$O_2 + e^- \rightarrow O_2^-$	[a]
		$O_2^- + e^- \rightarrow O_2^{2-}$	[a]

[a]The thermodynamic potential of this reaction strongly depends on the solvent used

electrolyte in the ORR has been summarized in Table 7.1. In electrochemical devices such as fuel cells and metal–air batteries, the 4-electron pathway is highly desirable.

The kinetics of the reactions presented in Table 7.1 depends on two factors: (1) the rate of the electrons that are transferred from the electrode to the reactant species and vice versa, and (2) the rate of mass transport on the surface of the electrode to displace the reaction products and feed on the reactant species.

The mass transport is relatively easy to control through the design of the cell and the selection of the materials for the fuel cell construction, while the electrons transfer is more complicated. The model of Julius Tafel (classic model) for the electrons transfer relates the reaction rate constant with the molecular structure of the reactants and the characteristics of the reaction medium [3]. However, the theory proposed by Gerischer is more suitable in electrochemical systems because it realizes the nanoscopic aspects with voltage–current variable [4]. This theory is based on determining the energy density states and their occupation in the electrode and the reactant species, associating the probability of tunneling between the electrode and the redox species.

Several studies about electron transfer have been performed by physicists [5, 6]. The main problem of electron transfer in solution is the highly polarizable environment in which transfer processes are carried out. The "polaron" theory has been discussed based on electron and hole conduction in semiconductors. The electron transfer occurs between one occupied quantum state and one quantum vacant state. During the ORR, the electron is transferred from the active site (occupied quantum state) to the oxygen molecule (vacant quantum state). In this case, the electrons in the electrode are studied according to the Sommerfeld–Drude model, while the electrons of the redox pair are treated as ions in solution.

In order to understand the fundamental about the effect of structure and properties of the non-noble metal electrocatalysts, several theoretical studies have been

developed [7]. Ab initio is considered a useful tool to calculate adsorption geometry, energy, the dissociation energy barrier, reversible potential, activation energy, and potential-dependent properties for elementary electron transfer steps [8]. In summary, the theoretical models have contributed greatly to the knowledge of the electrocatalytic systems and are considered a helpful tool for further development in this area.

Experimental studies are also widely used in the determination of some kinetical parameters of the ORR. The most frequently used techniques for the kinetic studies for the ORR are rotating disk electrode (RDE) and rotating-ring disk electrode (RRDE) . The ORR pathway is determined by RDE, and the number of electrons transferred is commonly calculated from the Koutecky–Levich plot [9], where the inverse of the kinetic current ($1/i_k$) is plotted versus the inverse of the square root of the rotation speed ($1/\omega^{1/2}$) according with the Koutecky–Levich Eq. (7.1):

$$\frac{1}{i} = \frac{1}{i_k} + \frac{1}{i_L} = \frac{1}{i_k} + \frac{1}{0.62\mathrm{nFAD}^{2/3}\mathrm{Cv}^{-1/6}w^{1/2}} \tag{7.1}$$

where i_k is the kinetic current for the ORR, i_L is the mass transport limiting current, n is the number of electrons per oxygen molecule for the ORR, F is the Faraday constant, A is the geometrical area of electrode, C is the saturation concentration for oxygen in water, D is the aqueous binary diffusion coefficient of oxygen, ν is the kinematic viscosity of the solution, and ω is the rotation rate.

Additionally, $1/0.62\mathrm{nFAD}^{2/3}\mathrm{Cv}^{-1/6}$ can be determined when calculating the Koutecky–Levich slope [10]. However, the Koutecky–Levich method was developed more than 50 years ago, under the assumptions of elementary reactions [11]. This method is not very useful with some of the recently developed nanostructured 3D electrocatalysts in alkaline electrolytes. Koutecky–Levich plots are often not linear and the electron number (n) sometimes exceeds the theoretical limits. It is highly desirable that the estimation of n, which is a very important indicator of the performance of an electrocatalyst, should preferably be performed with the RRDE technique. This technique allows the detection of intermediate compounds as H_2O_2 during the ORR, where n and the peroxide hydrogen percent are calculated from RRDE data using Eqs. (7.2) and (7.3) [12]:

$$n = \frac{4i_D}{i_D + i_R/N} \tag{7.2}$$

$$\%\mathrm{H_2O_2} = \frac{200i_R/N}{i_D + i_R/N} \tag{7.3}$$

where i_D is the reduction current density at the disc, i_R is the oxidation current density at the ring, and N is the collection efficiency of the RRDE.

The polarization curves that are typically obtained from the RRDE data are shown in Fig. 7.1a, where the current registers by the disk at several rotations rates are plotted. The ring current is several orders of magnitude smaller than the current of the disk (Fig. 7.1b). The plots of the Figs. 7.1c, d have been obtained from

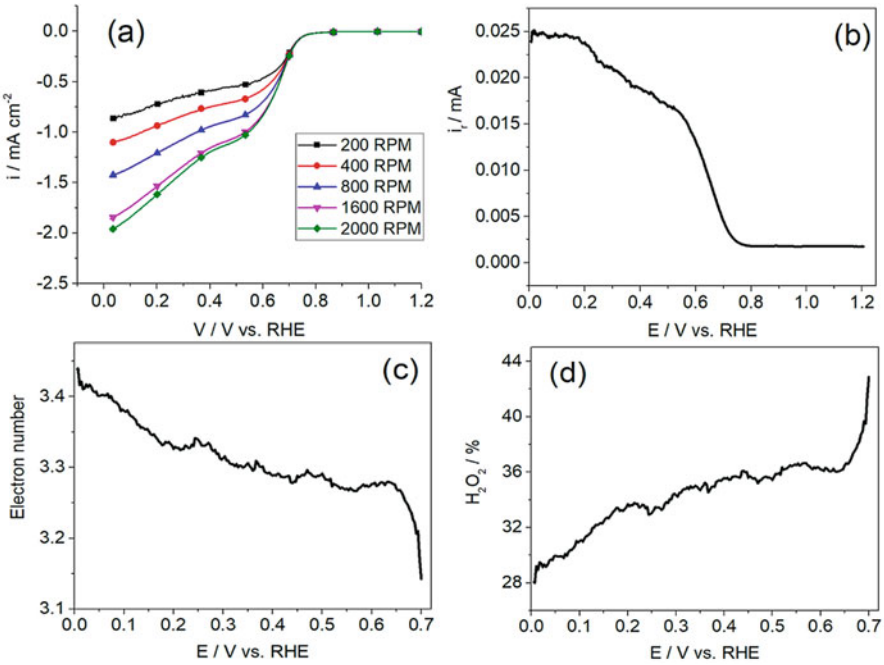

Fig. 7.1 Typical plots obtained from RDDE technique: (**a**) potential-current curves collected by the disk, (**b**) potential-current curve collected in the ring, (**c**) electron number n calculated from Eq. (7.2), and (**d**) H_2O_2% calculated from Eq. (7.3)

polarization curves data using the Eqs. (7.2) and (7.3). The number of electrons and the percentage of hydrogen peroxide can be calculated at different potentials. Thus, it is appreciated that *n* is not a constant value in the potential window of this test, as is assumed in Koutecky–Levich method; therefore, RDDE technique has important advantages to calculate *n*. In a study conducted by Zhou and coworkers [13], the authors suggest that it is preferable to use an electrode with Au ring instead of Pt, in addition to proposing an interesting methodology to calibrate the N value (efficiency of collection).

Many of the experimental and theoretical methods proposed currently base their models on Pt-based electrocatalysts to explain the electron transfer and pathway for the ORR. However, these models have not been so useful when trying to explain these two parameters in non-noble metal electrocatalysts. Therefore, it has been necessary to propose new models and mechanisms according to the nature and properties of each material.

In the following sections, two main groups of non-noble metal electrocatalysts are presented, highlighting some of their most important properties in relation to the ORR performance.

7.3 Electrocatalysts for ORR in Acid Media

7.3.1 Transition Metal Macrocycles

In recent years, transition metals macrocycles (TMM) are studied as alternative of Pt-based electrocatalyst, due they have a good catalytic activity for ORR in acid electrolytes. These materials are large molecules composed of a transition metal bound to a complex ligand. There are several reports in the literature about TMM that have been studied for the ORR. Some of these studies considered the use of noble transition metals such as Pd, Pt, or Ru [12]. However, in this chapter we will focus only on TMM with non-noble metals in their chemical structure.

The TMM with better performances and a remarkable electrocatalytic activity for the ORR are Fe- and Co- macrocyclic complex. Moreover, other TMM studied, although with less attractive performances, include transition metals such as Mo [14], Ni [15, 16], Cu [17, 18], Zn [16], Mn [19], V [16] and Ti [20].

Regarding the complex ligands, they play an important role maintaining stable the metal in the electrode surface and serving as active site. The chelating group composed of four nitrogen atoms (N_4) that coordinate with the metal ion for the TMM formation. Phthalocyanine (Pc) and porphyrin (PP) are the most used ligands complex in the literature. The structural formulas of the TMM with a Pc and PP ligands complex are shown in Fig. 7.2.

The reaction mechanism that takes place to carry out the ORR in these materials is still unclear. Several results from electrochemical studies suggest that electronic transfer occurs with the combination of 2- and 4-electron pathway. Some authors suggest that ORR involves a modified redox reaction [21, 22], where the first step involves the adsorption of O_2 on the metal ion located in the center of the TMM forming and oxygen–catalyst adduct. Subsequently, electrons are released and

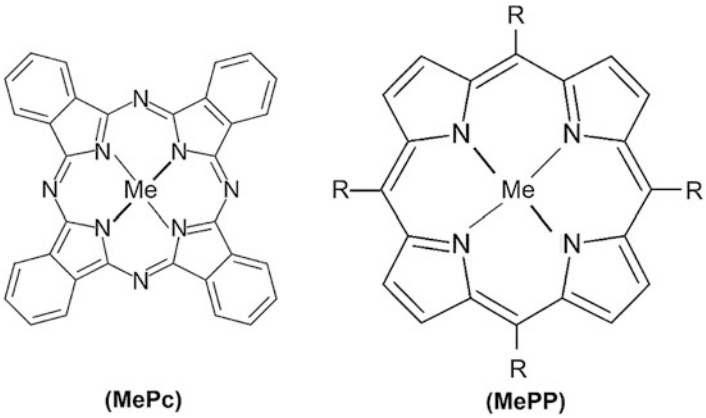

Fig. 7.2 Structural formula of TMM of the most reported ligands complex: phthalocyanine (Pc) and porphyrin (PP), Me = Transition metal ion and R = substituents

transferred from the metal ion to the bond of the oxygen molecule. The adduct undergoes further reductions forming intermediate spices like hydrogen peroxide or water. The reduced N_4-chelates will be regenerated to complete the cycle (Eqs. (7.4), (7.5), (7.6), and (7.7)).

$$XMe^{2+} + O_2 \rightarrow \left(XMe^{\delta+} \ldots {O_2}^{\delta-}\right) \tag{7.4}$$

$$\left(XMe^{\delta+} \ldots {O_2}^{\delta-}\right) + H^+ \rightarrow \left(XMe^{3+} \ldots O_2H\right)^+ \tag{7.5}$$

$$\left(XMe^{3+} \ldots O_2H\right)^+ + H^+ + e^- \rightarrow XMe + \text{intermediates (peroxide)} \tag{7.6}$$

$$H_2O_2 + XMe \rightarrow H_2O + 1/2\ O_2 \tag{7.7}$$

On the other hand, several factors have been identified that have a direct effect on the ORR activity such as the transition metal, the complex ligand, the heat treatment, and the support used.

The central transition metal defines largely the electron transfer pathway by which the ORR is carried out. It has been shown that most TMM with Fe reduce by direct 4-electron pathway, while TMM with Co generate peroxide as an intermediate product through the 2-electron pathway. However, Co complexes have shown more electrochemical stability than Fe complexes. Moreover, the formation of dimetal face-to-face macrocycles is another interesting alternative. An electrocatalyst with two Co centers face-to-face can provide two adsorption sites for O_2 molecule instead of one site promoting the 4-electron transfer process [23]. In addition, the advantage of combining two different metal centers with porphyrins complex ligand has been studied [16], resulting electrocatalysts with much greater activity and stability for ORR than electrocatalysts with a metal center only.

Furthermore, the complex ligand also plays an important role in the ORR. The majority complexes with Fe and Co have ORR activity, and their catalytic activity is attributed to the inductive and mesomeric effects of the ligand to the central metal ion [24]. Some of the N_4 chelate complexes evaluated for the ORR are tetracarboxyphthalocyanine (TcPc), tetramethoxyphenylporphyrin (TMPP), tetraphenylporphyrin (TPP), tetrasulfophthalocyanine (TSP), phthalocyanine (Pc), and dibenzotetraazaannulene (TAA).

The N_4 chelate complexes have their optimal catalytic activity when are subjected to heat treatments in a temperature range of 500–700 °C [16]. At temperatures below 500 °C, the catalytic activity is usually reduced by half, while at too high temperatures the active sites Me–N_4 are destroyed and lose their active nature [17]. Then, the effect of the heat treatment has a direct effect on the catalytic activity; however, it does not have a significant effect on the catalytic stability [12].

Jaouen et al. [25] suggest that the catalytic activity of Fe–N_4/C and FeN_2/C electrocatalysts depends directly on the type of carbon material in which they are supported. Specific surface area and pore size distribution are determining factors in the performance for the ORR. Although the most important factor is the nitrogen content in these materials, the higher it is, the higher is the density of the catalytic

sites. In terms of electrochemical parameters, the TMM performances report onset potentials in a range of 600–800 mV vs. RHE in strong acid electrolytes and current densities like the Pt-based electrocatalysts [26–29].

The ORR activity of TMMs has recently been evaluated in alkaline electrolytes; however, these results are not discussed in this review. If the reader is interested in this topic, there are several reviews that we recommend [30, 31].

The future research directions for the TMM as non-noble metal electrocatalyst request exploring new materials that optimize the catalytic activity and stability, may be optimizing the heat treatments in order to introduce more nitrogen active sites, using novel carbon supports with high surface areas and tunable pore sizes. Finally, the fundamental understanding of the reaction mechanisms involved in the ORR is necessary.

7.3.2 Transition Metal Chalcogenides

The pioneers in the development of transition metal chalcogenides (TMC) as non-noble metal alternative electrocatalysts are Alonso-Vante and Tributsch, publishing the first report three decades ago [32]. The TMC have a cluster structure with a repeating crystal lattice, the so-called Chevrel phase. The metal ion in the center is surrounded by several nonmetal ions. There are binary compounds with a basic formula Me_xX_y, where Me is a transition metal and X is chalcogen (e.g., S, Se, or Te). There are also ternary compounds with basic formula $MoM^1{}_xX_y$, where M^1 is an intercalated metal guest ion and the so-called pseudobinary compounds such as $MoM^2{}_xX_y$, where M^2 is a metal ion which replaces the Mo in the octahedral M^2 cluster.

Extensive studies have focused on Me_6X_8 and $MoM^2{}_xX_8$ pseudobinary compounds, due to their high current density and relative and comparatively close onset potential to platinum reported for the ORR. The reaction mechanism for an oxygen molecule in acid medium is proposed by Alonso-Vante [33]:

$$\bullet + O_2 \rightarrow \bullet - O_{2ads} \tag{7.8}$$

$$\bullet - O_{2ads} + (H^+ + e^-) \rightarrow \bullet - O_{ads} + H_2O \tag{7.9}$$

$$\bullet - O_{ads} + (H^+ + e^-) \rightarrow \bullet - OH_{ads} \tag{7.10}$$

$$\bullet - OH_{ads} + (H^+ + e^-) \rightarrow \bullet + H_2O \tag{7.11}$$

where the active site localized on the electrode surface is •, and an oxygen molecule adsorbed on an active site is $\bullet{-}O_2$. The ORR takes place with the transition metal d-states. For example, for the TMC $Mo_4Ru_2Se_8$, the catalytic center is the ruthenium atoms. For this material, the cluster serve as electrons reservoirs that adsorb oxygen molecules which favored the formation of water via 4-electron pathway. On the other hand, a change of volume occurs during the transfer process, which favors the

breaking bond O=O, and this last theory has been confirmed using nanodivided chalcogenide materials [34–37].

The carbonyl chemical route is the synthesis method most used to obtain TMC with Chevrel phase clusters. Ru_xSe_y electrocatalysts contain Ru *hpc* core cluster whose surface is coordinated to selenium atoms [34, 38–40], which preset a promising activity toward ORR and good methanol tolerance. Additionally, they can reduce oxygen by the 4-electron pathway.

Binary TMC containing Ru, Ir, Co, Fe, and Ni have shown high activity for the ORR [41–46], while the ternary Ru-Mo-Se TMC with Chevrel phase has been widely studied in this application [47]. Ru-based chalcogenides show high catalytic activity and good stability toward ORR in acid media. However, this noble metal and other such Ir-, Pt-, and Rh-based chalcogenides are not feasible for large-scale commercialization of PEMFC.

Regarding non-noble metal chalcogenide electrocatalysts, these have been reported since 1970. Combination of TMC consisting in Co_xS_y have high density current (958–2150 mA/m^2 at 5 0.0–0.6 V vs. RHE), good chemical stability, and an open circuit potential (OCP) $\approx$ 0.83 V vs. RHE [48], while the binary TMC containing Ti, W, Ta, Mo, and Cr bound to S atoms are shown the lowest current densities (> 1 mA/m^2 at 0.6 V vs. RHE). Furthermore, cobalt selenides supported on carbon ($Co_{1-x}Se/C$) exhibit significant ORR current compared with Co, Se, and carbon. The OCP in acid medium for these electrocatalysts is of 0.78 V vs. RHE [49]. In another research, Feng and coworkers investigated the ORR activity of $CoSe_2/C$; in this work, chalcogenide nanoparticles show an OCP of 0.81 V vs. RHE, and the electron transfer process involves about 3.5 electrons and the production of H_2O_2 between 15 and 30% (higher than the requirement below 5%) [50]. Although, one of the best performing TMCs is the pseudobinary compound $CoNiS_2$ with spinel structure and an OCP of 0.89 V vs. RHE.

Some theoretical studies have been carried out with the objective of clarifying the reaction mechanisms involved in the ORR. Sidik and Anderson conducted a study using the Vienna ab initio simulation package (VASP). They propose a mechanism of a TMC type Co_9S_8 with pentlandite structure, where the oxygen molecule can be adsorbed in a cobalt site or a sulfur site. In this work, they calculated the theoretical overpotentials between 0.74 and 0.89 V, which are higher compared to the overpotentials calculated for cobalt selenides with the same approach (0.22 V) [51].

There is still a long way to go to explore all the alternatives of TMC as non-noble metal electrocatalysts. The main challenges that they present are to improve their catalytic activity, which is still below that of Pt-based electrocatalyst. In addition, it is necessary to propose synthesis methods that are more environment friendly, using green solvents, for example. Finally, it is worth mentioning that in recent years there has not been an important development of TMC evaluated in acid medium; and that as with other types of materials such as TMM, the interest has focused on evaluating these materials in an alkaline medium.

7.3.3 Transition Metal Nitrides and Carbides

Transition metal nitrides (TMeN) and carbides (TMeC) have physical properties such as high melting point, high electrical conductivity, and chemical stability as well. These features make them excellent candidates as electrocatalysts to operate under the hostile conditions in the cathode of the fuel cells. The TMeC and TMeN are considered as "interstitial allows" [52] formed between transition metals of groups IVB-VIB and nitrogen or carbon atoms (see Table 7.2). Moreover, these materials are usually unstable with most of the metals of groups VIIB and VIIIB, mainly noble metals. An exception is the Fe, which can form iron carbides/nitrides (Fe_3C and Fe_3N), and Co and Ni, which can form nitrides such as Co_3N and Ni_3N, respectively.

TMeC and TMeN often have unit cells such as face-centered cubic (fcc), hexagon close-packed (hcp), and hexagonal simple, which are usually formed by the small carbon or nitrogen atoms occupying interstitial positions (Fig. 7.3) [53]. The intercalation of the nitrogen/carbon atoms in the metal lattice causes an expansion, which would be broadening the metal d-band. These contractions in the d-band produce a greater density of states (DOS). This redistribution of DOS could give to the carbides and nitrides electronic properties analogous to the noble metals [54]. However, theoretical models and catalytic mechanisms are still under discussion.

Despite the similarities in the electronic structure of carbides and nitrides compared to noble metals, their electrochemical activity toward the ORR is still low. The

Table 7.2 Transition metal carbides/nitrides and their formula regarding their position in the periodic table

	Group		
	IVB	VB	VIB
Carbides	TiC_{1-x}	VC_{1-x}	Cr_3C_2
	ZrC_{1-x}	NbC_{1-x}	Mo_2C
	HfC_{1-x}	TaC_{1-x}	WC
Nitrides	TiN	VN_{1-x}	Cr_3N_2
	ZrN_{1-x}	NbN_{1-x}	Mo_2N
	HfN_{1-x}	TaN_{1-x}	WN

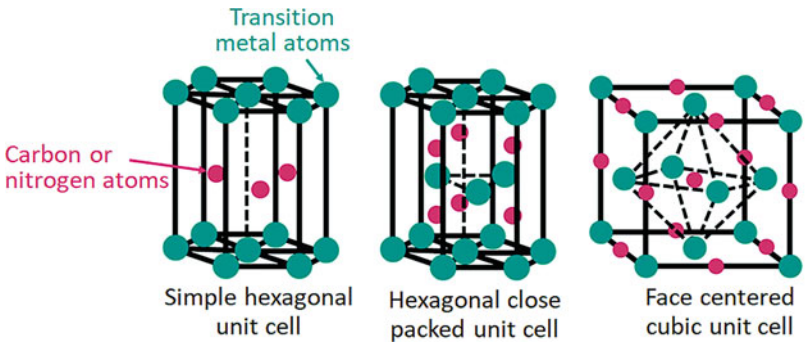

Fig. 7.3 Common unit cells of the TMeN and TMeC

WC, for example, is unstable at potentials over 0.6 V vs. RHE [55]. To improve its stability at higher potentials, Lee and coworkers synthesized the compound $W_{42}Ta_{24}C_{34}$, which is more stable in acid corrosive environments than WC and has an onset potential 350 mV higher than pure WC [56]. In other research, the addition of Ta to nickel carbide ($Ni_{33}Ta_{41}C_{26}$) had an effect like the mentioned above, where Ta improves the stability and onset potential of the electrocatalysts for the ORR; however, Ta_2O_5 is formed, which is a problem due that this oxide is an electrical insulation [57].

Recently, it was reported Fe_3C as novel non-noble metal electrocatalyst with high onset potential (0.92 V vs. RHE) and good stability in strong acid electrolytes [58]. Moreover, ternary Fe/N/C has been considered one of the most promising candidates for their high ORR activity [59–61]. The synergistic effect between Fe and N supported on carbon matrix promotes the ORR and is relatively stable in acidic media. Lui and coworkers [62] developed core shell Fe_2N/C structures from seaweed biomass, in which the nitride is the core and nitrogen-doped amorphous carbon is the shell. The ORR performance shows a high onset potential of 0.93 V vs. RHE in 1 M $HClO_4$ electrolyte, good tolerance to methanol, and an electron transfer number of 3.85.

Furthermore, monometallic (δ-MoN, Mo_5N_6, and Mo_2N) and bimetallic ($Co_{0.6}Mo_{1.4}N_2$) molybdenum nitrides exhibit catalytic activity with a modest onset potential of 0.71 V vs. RHE and electron transfer mechanism of 4-electron at potential lower than 0.5 V [63].

The reaction mechanisms of the ORR are not clear yet; however, it is evident that the synergy that occurs between Fe–C–N improves the catalytic activity. Thus, materials based on these elements are the most promising electrocatalysts to replace noble metal-based catalyst operating in acid media. Recently, Sun and coworkers achieve a comparative study between Fe_3C, Fe_2N, and Fe–N_4/C moieties. The highest catalytic activity of Fe–N_4/C moieties has an onset potential of 0.879 V vs. RHE. However, the formation of moieties is not easy to obtain. On the other hand, the catalytic activity of iron nitride/carbide is lower than moieties and they are unstable in acid media due to their possible dissolution [64].

7.4 Electrocatalysts for ORR in Alkaline Media

7.4.1 Perovskite-Type Oxides

Oxides with perovskite or closely related structures play an important role in the development of effective earth-abundant and low-cost electrocatalysts for renewable energy storage and conversion systems. Perovskite oxides obtain their name from the structure of the mineral calcium titanium oxide ($CaTiO_3$) discovered in 1839 [65].

Commonly, perovskites have the general chemical formula ABO_3, where A is a rare-earth, alkaline earth, or a mix of both cations and B is one or more transition metal cations [66, 67]. The ideal cubic perovskite lattice is shown in Fig. 7.4a, b. It

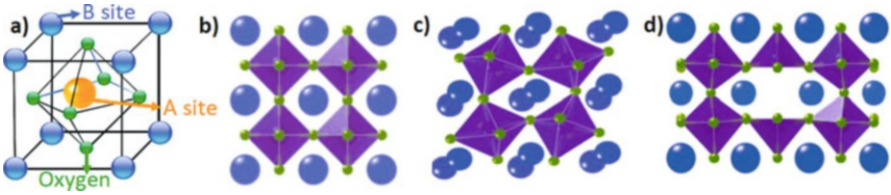

Fig. 7.4 (**a**, **b**) Ideal cubic perovskite unit cell. (**c**) Distorted perovskite structure and (**d**) perovskite structure with partial B-site substitution

consists of A cations located at the corners of the cube, which are 12-fold coordinated by oxygen. While cations at the B site are in the center, octahedrally coordinated with oxygen ions in the face-centered positions. The A site cation is slightly larger than B cation. The structure is commonly visualized as a three-dimensional network of regular corner-linked BO6 octahedra, where all B–O–B angles are 180°.

However, the wide variety of substitutions in the A and B sites lead to structural distortion and/or oxygen vacancies (δ) that can be related to the A and B ionic radii and electronic configuration of the metal ions. The degree of deviation from the ideal cubic perovskite can be quantified using the Goldschmidt tolerance factor (*t*) [68]. It relates how much strain can tolerate the lattice before it deforms. Thus, the perovskite-type structure is usually obtained in the range of $0.75 \leq t \leq 1.0$, for the ideal perovskite structure $t = 1$. The limiting values of t may differ depending upon the set of ionic radii employed [69]. As t decreases from 1 (A cations are too small), the perovskite structure deforms to orthorhombic or rhombohedral structures. When t is higher than 1 (A cations are very large), the structure of the perovskite is no longer cubic leading to a so-called hexagonal perovskite. In which, the octahedra share faces instead of corners modifying the M-O bond distances as well as making possible interactions between transition metals (Fig. 7.4c) [66, 69].

Moreover, it is possible to make partial substitutions of the A or B sites giving the formation of quaternary oxides or double perovskite. Where the cations in the A or B site are two different elements with strongly differing sizes $(A_xA'_y)BO_3$, $A(B_xB'_y)O_3$ where $x + y = 1$ or a complex perovskite $(A_xA'_y)(B_xB'_y)O_3$. These oxides result in a complex structure array and oxygen vacancies are frequently presented. Some of these oxides are known as perovskite-like oxides, see Fig. 7.4d. Interestingly, there is a relation between the structural distortions and oxygen vacancies (or oxygen nonstoichiometry δ) to the rise of important properties in the perovskite oxides. Thus, their physicochemical properties can be systematically tuned by carefully selecting the A or B cation and adjusting the stoichiometry [66, 69]. Up to now, many perovskite-type oxides and perovskite-like oxides have been generated and investigated as electrocatalysts for the ORR. They have shown promising electrocatalytic activity and stability in alkaline solutions due to their high electrical conductivity and outstanding catalytic behavior [66, 70, 71].

It was reported in the literature that for the ORR attractive electrocatalytic performance has been reported for perovskites containing in the A-site La, Nd, Ca, Sm, Li, Ba, and Sr ions and good chemical stability is obtained when Co, Fe, Mn, Ni,

and Cu ions were used at the B-site [66]. Among perovskite oxides, the lanthanum-based oxides have been recognized as one of the most promising electrocatalysts for the ORR. This type of oxides has high electrical conductivity at room temperature and significant stability against anodic oxidation in alkaline solution. Sunarso et al. [70] studied the electrocatalytic tendency of B-site substitution by the trivalent 3d transition metal ions such as Ni, Co, Fe, Mn, and Cr in $LaBO_3$ perovskite using a 0.1M KOH solution. The $LaCoO_3$ showed the largest ORR current density and the most positive onset potential followed by Mn, Fe, Ni, and Cr. Similar results were reported by Suntivich et al. [72] and Celorrio et al. [71] confirming that Co and Mn cations at the B-site presented the best performance for the ORR on $LaBO_3$ (B = Cr, Co, Fe, Mn, and Ni) nanoparticles. For these La systems, the ORR followed a close four-electron pathway.

Partial substitutions of the B site and stoichiometry on the electrocatalytic activity were studied by Larsson and Johansson [73] in $LaMn_xCu_yO_3$, $LaMn_xCr_yO_3$, and $LaMn_xNi_yO_3$ where $x = 0.1$–0.9 using 6 M KOH solution. They tried to find a relation with the current density and the magnetic moment of the superoxide ion O^{2-} due to that the rate determining step in alkaline media involves the adsorption of the ion at the surface. However, they did not find a linear trend between the measurements. It is also known that for many perovskites charge ordering effects lead to charge disproportionation, but complementary spectroscopic experiments are required to understand the effect. Suntivich et al. [72] concluded that Mn is a more active element than Ni in the La oxides perovskites with partial substitution at the B-site.

The effect of A-site substitution on the ORR in an $AMnO_3$ was systematically varied using several lanthanoids and yttrium [74]. It was reported that the electrocatalytic activity is higher as the ionic radius of the lanthanide increases being in the order of La > Pr > Nd > Sm > Gd > Y > Dy > Yb. Partial substitutions at the A-site have been also studied for the system $AMnO_3$ using cations such as: $A = La_XCa_{1-x}$ where $X = 0.36, 0.4, 0.5, 0.6, 0.81$ [72, 75, 76]. $A = La_{1-x}Sr_x$, where $X = 0.1, 0.2, 0.33, 0.4, 0.5, 0.7, 0.8$ [77, 78]. In all studies, the best performance was obtained around 0.4 of the divalent A-site cation, which promotes the maximum oxidation state of Mn increasing the electron transfer number close to four. A similar tendency was obtained for the $Pr_{1-x}Ca_xMnO_3$ perovskite where the maximum current density was obtained when $x = 0.4$ [79].

Another important factor in the design of perovskite oxides for the ORR is the effect of oxygen stoichiometry. Several authors have reported that the appropriated amount of oxygen ion vacancies (δ) enhanced the electrocatalytic activity. Takeda et al. [80] found that for the $SrFeO_{3-\delta}$, the samples with $0.24 < \delta < 0.29$ showed the best activity. However, a slight dependence was observed in $SrCoO_{3-\delta}$. Du et al. [81] studied the effect of oxygen vacancies in the range of $0 < \delta \leq 0.5$ for the $CaMnO_{3-\delta}$, and the higher electroactivity was obtained when δ is close to 0.5 and average Mn valence close to 3.5. The improvement in the catalytic activity of the ORR is due to an rise electrical conductivity generated by the oxygen defects which facilitated the oxygen activation. The absence of too much oxygen will result in the formation of less conductive and poorly active perovskite oxide and the loss of perovskite structure.

Moreover, for the electrocatalytic measurements, perovskite oxides are usually mixed with carbon forming an electrocatalytic layer. It has been reported that the use of carbon disperses the oxide particles, electrically connects the particles, and enhances the electroactivity acting as cocatalyst in some cases. To investigate the effect of the amount of carbon in the electrocatalyst layer, Poux et al. [82] evaluated the electrocatalytic activity for the ORR on electrodes containing perovskite alone ($LaCoO_3$ and $La_{0.8}Sr_{0.2}MnO_3$), carbon alone, and both perovskite and carbon. They concluded that the presence of carbon electrocatalyzes the reduction of O_2 into OH^- as intermediate, which can react to ultimately result in a $4e^-$ ORR to water. Mixing it with perovskites improves the electrical contact between the oxide particles increasing the number of accessible active sites on the oxide surface for the reduction of the OH^{2-}.

Significant progress has been made over the last decades in understanding the electrocatalytic activity and stability of perovskite oxides for the ORR. The flexibility in the oxidation states leads to the formation of redox coupes, unique electronic properties, defective structure for oxygen vacancies or excess, and cation ordering resulting in distortion-free channels of oxygen vacancies and enhanced mobility of oxygen ions, which facilitate their bifunctional electrocatalytic activity for the oxygen reduction and oxygen evolution reactions. However, they can only be used in alkaline media, thus the long-term stability still being an issue to overcome. The formation of hydrogen peroxide during the ORR process can attack the electrocatalysts damaging their actives sites. Moreover, the structures of such active sites are not well understood. More research is necessary with emphasis on the activity–stability improvement. Further efforts are also required to understand the dependence of carbon supports and perovskites to catalyze the ORR or the use of other types of cocatalysts for engineering optimization proposes and fuel cell commercialization.

7.4.2 Spinel-Type Oxides

Spinel-type oxides are an interesting class of compounds that have been identified as promising candidates and alternatives to noble metal electrocatalysts. These oxides are also bifunctional electrocatalysts of the ORR and OER (oxygen evolution reaction) in alkaline media [83]. Spinel oxides with general formula AB_2O_4 are a very large family of compounds with the same crystal structure as the mineral $MgAl_2O_4$. The spinel structure can be described as a face-centered cubic close-packed array of O^{2-} ions, with tetrahedrally A^{2+} and octahedrally B^{3+} coordinated metal cations, see Fig. 7.5 [84]. Tetrahedral interstices are usually smaller than the octahedral; thus, cations with smaller ionic radii occupy the A-sites, while the larger cations occupy the B-sites. Moreover, to keep the valence balance, cation A can be in the $+2$ or $+$ 4 oxidation states and the corresponding cation B can be in the $+3$ or $+$ 2 oxidation states.

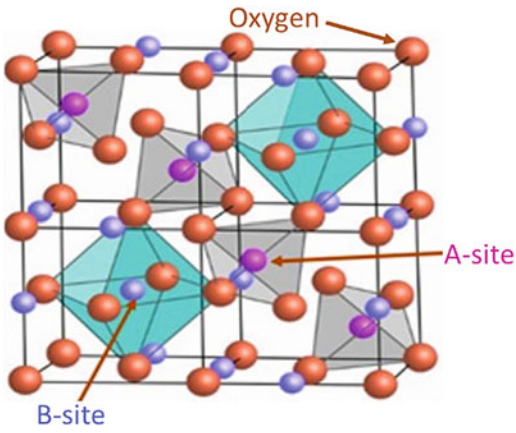

Fig. 7.5 Unit cell of ideal spinel-type oxide structure

The variations in distribution of cations in the A and B sites cause marked changes in some of the physical properties. For these oxides, several researches have been done to identify the active site and defect features, and understand the composition-dependent activities and intentional substitution of cations or dopants to enhance the electrocatalytic activity for the ORR [85–87]. Spinel oxides with cations on the B-site such as Co, Mn, and Fe are among the most active for the ORR. Many spinel oxides have been synthesized using cations in the A-site such as Co, Ni, Mn, Li, Zn, Cu, and Fe [83, 87].

In general, these compounds exhibit comparable electrocatalytic activities than precious metal-based electrocatalysts, high corrosion resistance, and easy availability. However, their low electrical conductivity and large particle size have limited their electrocatalytic performance and long-term stability. Numerous researches have been conducted to enhance their performance by controlling composition, designing nonstoichiometric oxides, creating defects, nanostructured characteristics, and using carbon nanomaterials as supports [87–90].

The synthesis of nonstoichiometric compounds and the creation of oxygen defects optimize the electronic structures of spinel, produce more active sites for molecular adsorption of oxygen, and reduce the reaction energy barriers. To examine the effect of M^{2+} substitution, Mn, Fe, Co, and Cu were used as cations in the nonstoichiometric $MFe_{3-x}O_4$. It was demonstrated that the most active spinel for ORR was $MnFe_{3-x}O_4$ followed by $Co_xFe_{3-x}O_4$, $CuxFe_{3-x}O_4$, and Fe_3O_4 [91]. Recently, Wei et al. [83] reported an increasing activity for $MnCo_2O_4$ with the reduction from $Mn^{3.7+}$ to $Mn^{3.2+}$ showing that the band gap occupancy of the active cation in the octahedral site is the activity descriptor for ORR, consolidating the role of electron orbital filling in metal oxide electrocatalysts.

Spinel with nanostructured characteristics as nanoparticles, nanoneedles, nanopetals, core-shell arrays, or porous structures have been prepared to improve their ORR properties. Zhu et al. [91] have been reported that $MnFe_2O_4$ nanoparticles (around 10 nm) with catalytic activity towards ORR comparable with the commercial Pt-based electrocatalyts in alkaline solution. The mesoporous nanostructured

MFe_2O_4 (M = Co, Mn, Ni) oxides exhibited excellent performance as bifunctional electrocatalysts for ORR and OER; the $CoFe_2O_4$ and $NiFe_2O_4$ exhibited higher OER activity than $MnFe_2O_4$ [89]. Recently, Bhandary et al. [92] synthesized $MnFe_2O_4$ nanopetals on porous carbon paper, and reported that electrocatalytic activity for the ORR (onset potential of 1.6 V vs RHE and higher current density of 11.5 mA/cm^2 at 2.0 V vs RHE reference electrode) was better than those other earlier reported spinel electrocatalysts and comparable to those spinel oxides supported on graphene or carbon nanotubes.

Carbon substrates are used to improve the electrical conductivity and adsorption capability by increasing the number of active sites. A high ORR electrocatalytic performance and durability was reported in a zinc ferrite/reduced graphene oxide ($ZnFe_2O_4$/rGO) with 69.8 wt.% of electrocatalyst, which follows a four-electron transfer mechanism in alkaline media [90].

7.4.3 Heteroatom-Doped Carbon Materials

Carbon materials are most widely used as electrodes in several energy devices such as fuel cell, batteries, and supercapacitors. In addition, they are frequently used as supports for many of the materials that have been mentioned in the previous sections. Certainly, this group of materials is one of the most promising for the performance of the ORR. Its boom began in 2009, when Dai et al. [93] reported that carbon nanotubes doped with nitrogen had high catalytic activity for the ORR in alkaline solution.

Basically, heteroatom-doped carbons are materials formed mainly by carbon atoms (<80% wt.), where doping consists in substituting a carbon atom with a heteroatom (N, S, B, P, etc.). The incorporation of one type of heteroatom into the carbon lattice generates a charge delocalization in the adjacent carbons, which promotes the formation of catalytic sites [94–96]. Additionally, the electronegativity and size of the doping atom has a determining influence on the electronic modulation of the electrocatalysts [97]. Moreover, it has been reported that the incorporation of dual-doped or more types of heteroatoms into carbon materials favors the formation of active sites, and usually have greater activity than its counterpart with a single heteroatom, and in some cases better catalytic activity than Pt/C [98–101]. In addition, most of these electrocatalysts have shown greater stability than Pt/C [102].

Nitrogen-doped carbons are probably the metal-free electrocatalysts most studied in the last decade [103–106]. Nitrogen–carbon bonds (N–C) can be identified relatively easily by X-ray photoelectron spectroscopy (XPS). Figure 7.6 shows the main N–C bonds in relation to their binding energy. This classification considers five types of N–C bonds commonly identified as pyridinic (N1), amine (N2), pyrrolic (N3), graphitic (N4), and pyridine-N-oxide (N5). Usually, several authors do not report the amine bond (N2, ≈399.4 eV); however, it has been reported that N2 bond is important to explain the evolution of carbon functionalities during pyrolysis treatments, to which carbon materials are usually subjected [107].

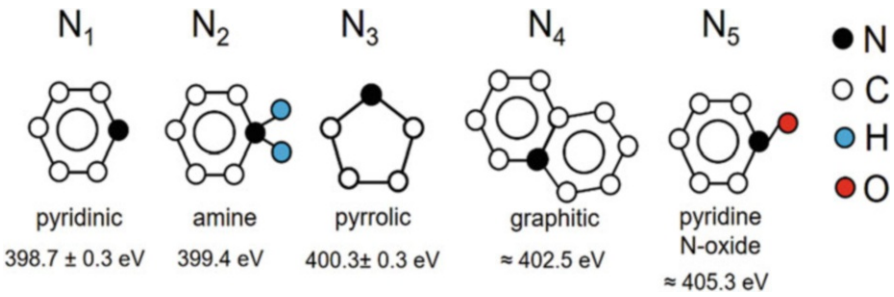

Fig. 7.6 Commonly nitrogen–carbon bonds identified by XPS in nitrogen-doped carbon materials

N-C type bond has a direct influence on the electrochemical performance of the electrocatalyst. Several studies suggest that N1 and N4 bonds favor the ORR [108]. However, the reaction mechanisms have not yet been fully elucidated. Conversely, it is currently a challenge to clarify these mechanisms and validate them experimentally and theoretically. Theoretical methods based on the density functional theory (DFT) have been widely used to propose some mechanisms. Some hybrid methods such as B3LYP-DFT and Car–Parrinello molecular dynamic simulation have also been employed [109, 110]. It should be noted that the theoretical studies proposed recently have been developed for nanostructured carbon materials such as carbon nanotubes and graphene doped with nitrogen.

Zhang and Xia [111] reported a theoretical study, where they justify how the ORR takes place for 4-electron pathway in N-doped graphene, and this reaction did not arise in pristine graphene, due mainly to pristine graphene does not have electroactive sites. Additionally, they observe that when introducing hydrogen atoms at the edges of the carbon lattice, the sequential reactions for the ORR energetically can occur. One of these reactions involves the formation of the chemical bond O–C between the oxygen of the medium and one carbon of the graphene. The O–O bond breaks up forming water molecules. For each step of the reaction, the energy of the system decreases, which indicates that the reaction by 4-electron pathway is spontaneous and possible. The active catalytic sites depend on the distribution of the density of the spin and the distribution of the atomic charge. The substitution of nitrogen atoms generates a pair of free electrons that modifies the distribution of the atomic charge in graphene. According to this study, carbon atoms with high spin densities are the electrocatalytically most active sites. As can be expected, N–C bond type has influence in the charge distribution of the carbon atoms adjacent to where the nitrogen doping atom is located. The dopant or heteroatom that is introduced into the carbon lattice not only causes changes in the distribution of electronic charge, it also causes defects such as bending and breaking of C–C bonds in the lattice.

The catalytic activity toward ORR for N-doped carbon materials is close to Pt/C electrocatalyst; however, the cost of these metal-free electrocatalysts is considerably lower, which opens the possibility of large-scale production of the fuel cells. Many reports show that N-doped carbons have onset potential in a range of 0.75 to

0.86 V vs. RHE. For example, partially exfoliated N-CNT has onset potential of 0.77 V [112]. Moreover, N-doped graphene synthetized by resin-based methodology has an onset potential 60 mV lower than Pt/C, comparable activity but higher durability than Pt/C, and 3.9 electron transfer number at −0.2 V [113]. Other authors have obtained N-doped graphene with promising performance, and most of them agree that these metal-free electrocatalysts have comparable ORR activity with Pt/C, higher long-term stability and resistance to crossover than Pt/C [103, 114–116].

Besides nitrogen, nanostructured carbon materials as carbon nanotubes (CNT), graphene, mesoporous ordered carbons (MOC), carbon aerogels, and carbon nanofibers (CNF) have been doped with heteroatoms such as sulfur [117–119], boron [120–122], phosphorous [123, 124], silicon [125], and halogens [126, 127].

Table 7.3 summarizes several heteroatom-doped nanostructured carbons evaluated as metal-free electrocatalysts in alkaline electrolyte, the range of binding energy in which they are usually identified by XPS, the type of bond formed between heteroatom-carbon and other elements that usually are present, and their onset potential according to recent reports. It should be noted that for comparative purposes, it is best to report the onset potential vs. the reversible hydrogen electrode (RHE), because the pH of the electrolyte is adjusted.

Table 7.3 Chemical structure of some heteroatom-doped carbon nanostructured electrocatalysts and their electrochemical activity toward the ORR

Heteroatom	Energy binding (eV)	Formed bonds	Onset potential	Reference
Si 2p	100–105	SiO_2 C–Si–O Si–C	−0.2 V vs. Ag/AgCl in 0.1 M KHO	[125]
P 2p	132–137	P–C P–O P=O	−0.2 V vs. Hg/Hg_2Cl_2 in 0.1 M KOH	[123]
S 2p	161–172	C–S–C R–SO_2 RO_2–S–S–R	0.69 V vs. RHE 0.88 V vs. RHE 0.86 V vs. RHE 0.96 V vs. RHE 0.80 V vs. RHE	[128] [129] [130] [131] [132]
B 1s	186–194	B_2O_3 CBO_2 C_2BO B–C sp^2 B_4C	0.83 V vs. RHE −0.14 V vs. Ag/AgCl in 0.1 M KOH	[122] [121]
I 3d	617–632	I2 I–C	≈ −0.1 V vs. Ag/AgCl in 0.1 M KOH	[127]
F 1s	681–690	Ionic C–F Semi-ionic C–F Covalent C–F	≈ −0.15 V vs. SCE in 0.1 M KOH ≈ −0.13 V vs. SCE in 0.1 M KOH	[133] [126]

It can be seen that heteroatom-doped nanostructured carbon shows promising performances toward the ORR. However, nanostructured carbon materials currently have several drawbacks: (1) the chemical reagents used in the processes to obtain them, generally they are of high purity and high costs, which in many cases are hazardous for the health and the environment; (2) although sophisticated technologies or equipment are used in synthesis processes, even large-scale production remains a challenge in order to obtain high quality materials [134].

The most recent research has a clear tendency: to use natural sources of carbon and heteroatoms as raw materials instead of expensive reagents that are commonly hazardous chemicals, mainly motivated by economic and environmental reasons [135]. In addition, several investigations have been carried out proposing less inexpensive methodologies to obtain nanostructured carbon materials and increase the large-scale production [134, 135]. The use of biomass as a carbon and heteroatom source to obtain metal-free electrocatalysts is economically and environmentally attractive. This alternative has recently been explored; biomass-derived electrocatalysts have performance for the ORR higher than heteroatom-doped nanostructured carbons, and in some cases higher than Pt/C. Most of the biomass waste is usually used as an energy source through direct combustion and gasification processes, among others. However, the possibility of taking advantage of biomass residues for the manufacture of carbon materials used in electrochemical devices is very attractive. In addition, the technology to obtain them is inexpensive [136–138]. The above, then, also represents an alternative for the exploitation of several biomass wastes generated in large quantities and that are currently disposed in landfills or are left open.

Food and several biomass wastes such as urban, forest, vegetable, and animal wastes have been used as raw materials in obtaining metal-free electrocatalysts. Most biomass-derived carbons are synthetized by pyrolysis and/or hydrothermal carbonization treatments. Their electrochemical performances are very attractive; for example, egg [139], soybeans [140], amaranth [141], soy milk [142], and honey [143] have been used as raw materials in obtaining metal-free electrocatalysts and evaluated in the ORR.

However, the use of food in obtaining carbon could have serious food implications globally. Plant and forest wastes such as tree leaves [144], vegetables skin [128], luffa [145], and algae [146, 147] have also been explored to obtain metal-free electrocatalysts. As far as animal waste is concerned, carbons have been obtained from human hair [148], human urine [149], leather [137, 138], bones, and pig blood [150, 151]. Generally, the electrochemical performance of these materials in an alkaline media is comparable to that of Pt/C, due to their high surface areas, and high current densities are usually reported. However, it is still a challenge to improve the onset potential.

7.5 Conclusions

Throughout the last decade, a wide variety of materials have been studied as non-noble metal electrocatalysts, each family of materials have advantages and disadvantages over Pt/C. However, to have electrocatalysts with the most favorable properties for ORR, it is necessary to use several types of materials to enhance their properties. On the other hand, carbon materials have been used as a support and as metal-free electrocatalysts, they are very versatile materials, of great abundance and therefore of low cost. Prospects indicate that heteroatom-doped carbon materials in combination with transition metals such as Fe or Co could be a very promising option for the substitution of noble metals in fuel cell cathodes.

Now, environmentally the use of biomass waste as raw material for producing metal-free electrocatalysts would be very attractive. The main advantage of these materials is that they have a heterogeneous chemical composition, which includes metals that can function as active sites for the ORR. There is still a long way to go to develop a material with the properties to replace the noble metals; however, the use of non-noble metal electrocatalysts is a research area that is developing rapidly. Last, but not least, it must be considered that for the development of new non-noble metal electrocatalysts it is necessary to implement methodologies that have a low environmental impact; in addition, the process must be easily scalable to cover market demand and that its production involves the use of technologies of easy implementation.

Acknowledgment The authors would like to thank to the Mexican Council for Science and Technology (CONACyT) for financial support grant CB-2015-250632.

References

1. Shao M, Chang Q, Dodelet J-P, Chenitz R (2016) Recent advances in electrocatalysts for oxygen reduction reaction. Chem Rev 116:3594–3657
2. Zhang L, Zhang J, Wilkinson DP, Wang H (2006) Progress in preparation of non-noble electrocatalysts for PEM fuel cell reactions. J Power Sources 156:171–182
3. Allen J, Bard LRF (2000) Electrochemical methods: fundamentals and applications, 2nd edn. Wiley, New York
4. Gerischer H (1997) Principles of electrochemistry. In: Gellings PJ, Bouwmeester HJM (eds) The CRC handbook of solid state electrochemistry, 1st edn. CRC Press, Boca Raton, p 656
5. Adzic R, Gong K (2017) Platinum-monolayer oxygen-reduction electrocatalysts: present status and future prospects. In: Mirking MV, Amemiya S (eds) Nanoelectrochemistry, 1st edn. CRC Press, Pittsburgh, pp 125–144
6. Soldano GJ, Schmickler W, Juarez MF, Quaino P, Santos E (2017) Electron transfer in nanoelectrochemical systems. In: Mirking MV, Amemiya S (eds) Nanoelectrochemistry, 1st edn. CRC Press, Pittsburgh, pp 3–28
7. Dy E, Shi Z (2014) Theoretical modeling of non-noble metal electrocatalysts for acid and alkaline PEM fuel cells. In: Chen Z, Dodelet J, Dodelet JZ (eds) Non-noble metal fuel cell catalysts. Wiley, Weinheim, pp 205–242

8. Shi Z, Zhang J, Liu ZS, Wang H, Wilkinson DP (2006) Current status of ab initio quantum chemistry study for oxygen electroreduction on fuel cell catalysts. Electrochim Acta 51:1905–1916
9. Koutecky J, Levich BG (1958) The application of the rotating disc electrode to studies of kinetic and catalytic processes. Zhurnal Fiz Khimii 32:1565–1575
10. Zhang HJ, Yuan X, Sun L, Zeng X, Jiang QZ, Shao Z, Ma ZF (2010) Pyrolyzed CoN4-chelate as an electrocatalyst for oxygen reduction reaction in acid media. Int J Hydrog Energy 35:2900–2903
11. Frumkin A, Nekrasov L, Levich B, Ivanov J (1959) Die anwendung der rotierenden scheibenelektrode mit einem ringe zur untersuchung von zwischenprodukten elektrochemischer reaktionen. J Electroanal Chem 1:84–90
12. Song C, Zhang J (2008) Electrocatalytic oxygen reduction reaction. In: Zhang J (ed) PEM fuel cell electrocatalysts and catalyst layers: fundamentals and applications. Springer, London, pp 89–134
13. Zhou R, Zheng Y, Jaroniec M, Qiao S-Z (2016) Determination of the electron transfer number for the oxygen reduction reaction: from theory to experiment. ACS Catal 6:4720–4728
14. Xia D, Liu S, Wang Z, Chen G, Zhang L, Zhang L, Hui S (Rob), Zhang J (2008) Methanol-tolerant MoN electrocatalyst synthesized through heat treatment of molybdenum tetraphenylporphyrin for four-electron oxygen reduction reaction. J Power Sources 177:296–302
15. Behret H, Binder H, Sandstede G, Scherer GG (1981) On the mechanism of electrocatalytic oxygen reduction at metal chelates. J Electroanal Chem Interfacial Electrochem 117:29–42
16. Chu D, Jiang R (2002) Novel electrocatalysts for direct methanol fuel cells. Solid State Ionics 148:591–599
17. Ding L, Xin Q, Dai X, Zhang J, Qiao J (2013) Evaluation of carbon-supported copper phthalocyanine (CuPc/C) as a cathode catalyst for fuel cells using Nafion as an electrolyte. Ionics (Kiel) 19:1415–1422
18. Reis RM, Valim RB, Rocha RS, Lima AS, Castro PS, Bertotti M, Lanza MRV (2014) The use of copper and cobalt phthalocyanines as electrocatalysts for the oxygen reduction reaction in acid medium. Electrochim Acta 139:1–6
19. Domínguez C, Pérez-Alonso FJ, Abdel Salam M, Gómez De La Fuente JL, Al-Thabaiti SA, Basahel SN, Peña MA, Fierro JLG, Rojas S (2014) Effect of transition metal (M: Fe, Co or Mn) for the oxygen reduction reaction with non-precious metal catalysts in acid medium. Int J Hydrog Energy 39:5309–5318
20. Demir F, Erdoğmuş A, Koca A (2013) Oxygen reduction reaction catalyzed with titanyl phthalocyanines in nonaqueous and aqueous media. Phys Chem Chem Phys 15:15926
21. Beck F (1977) The redox mechanism of the chelate-catalysed oxygen cathode. J Appl Electrochem 7:239–245
22. Zagal JH (1992) Metallophthalocyanines as catalysts in electrochemical reactions. Coord Chem Rev 119:89–136
23. Coliman JP, Denisevich P, Konai Y, Marrocco M, Koval C, Anson FC (1980) Electrode catalysis of the four-electron reduction of oxygen to water by dicobalt face-to-face porphyrins. J Am Chem Soc 102:6027–6036
24. Li J, Wu X, Yuan R, Lin H, Yu R (1994) Cobalt phthalocyanine derivatives as neutral carriers for nitrite-sensitive poly(vinyl chloride) membrane electrodes. Analyst 119:1363
25. Jaouen F, Marcotte S, Dodelet JP, Lindbergh G (2003) Oxygen reduction catalysts for polymer electrolyte fuel cells from the pyrolysis of iron acetate adsorbed on various carbon supports. J Phys Chem B 107:1376–1386
26. Baranton S, Coutanceau C, Garnier E, Léger J-M (2006) How does α-FePc catalysts dispersed onto high specific surface carbon support work towards oxygen reduction reaction (orr)? J Electroanal Chem 590:100–110

27. Faubert G, Côté R, Guay D, Dodelet JP, Dénès G, Poleunis C, Bertrand P (1998) Activation and characterization of Fe-based catalysts for the reduction of oxygen in polymer electrolyte fuel cells. Electrochim Acta 43:1969–1984
28. Sirk AHC, Ampbell SA, Birss VI (2005) Oxygen reduction by sol derived [Co, N, C, O]-based catalysts for use in proton exchange membrane fuel cells. Electrochem Solid-State Lett 8:A104
29. Alves MCM, Tourillon G (1996) Influence of complexation processes on the catalytic properties of some polymer-based cobalt compounds for oxygen electroreduction. J Phys Chem 100:7566–7572
30. Liu Y, Yue X, Li K, Qiao J, Wilkinson DP, Zhang J (2016) PEM fuel cell electrocatalysts based on transition metal macrocyclic compounds. Coord Chem Rev 315:153–177
31. Masa J, Ozoemena K, Schuhmann W, Zagal JH (2012) Oxygen reduction reaction using N_4-metallomacrocyclic catalysts: fundamentals on rational catalyst design. J Porphyr Phthalocyanines 16:761–784
32. Vante NA, Tributsch H (1986) Energy conversion catalysis using semiconducting transition metal cluster compounds. Nature 323:431–432
33. Alonso-Vante N, Fieber-Erdmann M, Rossner H, Holub-Krappe E, Giorgetti C, Tadjeddine A, Dartyge E, Fontaine A, Frahm R (1997) The catalytic centre of transition metal chalcogenides vis-à-vis the oxygen reduction reaction: an in situ electrochemical EXAFS study. J Phys IV 7: C2-887–C2-889
34. Colmenares L, Jusys Z, Behm RJ (2007) Activity, selectivity, and methanol tolerance of Se-modified Ru/C cathode catalysts. J Phys Chem C 111:1273–1283
35. Malakhov IV, Nikitenko SG, Savinova ER, Kochubey DI, Alonso-Vante N (2002) In situ EXAFS study to probe active centers of ru chalcogenide electrocatalysts during oxygen reduction reaction. J Phys Chem B 106:1670–1676
36. Alonso-Vante N, Malakhov I, Nikitenko S, Savinova E, Kochubey D (2002) The structure analysis of the active centers of Ru-containing electrocatalysts for the oxygen reduction. An in situ EXAFS study. Electrochim Acta 47:3807–3814
37. Alonso-Vante N, Borthen P, Fieber-Erdmann M, Strehblow H-H, Holub-Krappe E (2000) An in situ grazing incidence X-ray absorption study of ultra thin RuxSey cluster-like electrocatalyst layers. Electrochim Acta 45:4227–4236
38. Liu G, Zhang H, Hu J (2007) Novel synthesis of a highly active carbon-supported $Ru_{85}Se_{15}$ chalcogenide catalyst for the oxygen reduction reaction. Electrochem Commun 9:2643–2648
39. Zehl G, Schmithals G, Hoell A, Haas S, Hartnig C, Dorbandt I, Bogdanoff P, Fiechter S (2007) On the structure of carbon-supported selenium-modified ruthenium nanoparticles as electrocatalysts for oxygen reduction in fuel cells. Angew Chem Int Ed Engl 46:7311–7314
40. Delacôte C, Bonakdarpour A, Johnston CM, Zelenay P, Wieckowski A (2009) Aqueous-based synthesis of ruthenium–selenium catalyst for oxygen reduction reaction. Faraday Discuss 140:269–281
41. Feng Y, Alonso-Vante N (2008) Nonprecious metal catalysts for the molecular oxygen-reduction reaction. Phys Status Solidi 245:1792–1806
42. Alonso-Vante N (2011) 5 structure and reactivity of transition metal chalcogenides toward the molecular oxygen reduction reaction. In: Vayenas CG (ed) Interfacial phenomena in electrocatalysis. Springer, New York, pp 255–300
43. Satoshi Kaneco BV, Funasaka K (2006) Photo/electrochemistry and photobiology in the environment energy and fuel. Research Signpost, Trivandrum
44. Feng Y, Gago A, Timperman L, Alonso-Vante N (2011) Chalcogenide metal centers for oxygen reduction reaction: activity and tolerance. Electrochim Acta 56:1009–1022
45. Lee J-W, Popov BN (2007) Ruthenium-based electrocatalysts for oxygen reduction reaction-a review. J Solid State Electrochem 11:1355–1364
46. Gao M-R, Jiang J, Yu S-H (2012) Solution-based synthesis and design of late transition metal chalcogenide materials for oxygen reduction reaction (ORR). Small 8:13–27
47. Alonso-Vante N (2003) Vielstich W, Lamm A, Gasteiger HA (eds) Handbook of fuel cells: fundamentals, technology, and applications, 2nd edn. Wiley, New York, pp 534–543

48. Lee K, Alonso-Vante N, Zhang J (2014) Transition metal chalcogenides for oxygen reduction electrocatalysts in PEM fuel cells. In: Non-noble metal fuel cell catalysts. Wiley, Weinheim, pp 157–182
49. Susac D, Sode A, Zhu L, Wong PC, Teo M, Bizzotto D, Mitchell KAR, Parsons RR, Campbell SA (2006) A methodology for investigating new nonprecious metal catalysts for PEM fuel cells. J Phys Chem B 110:10762–10770
50. Feng Y, He T, Alonso-Vante N (2009) Oxygen reduction reaction on carbon-supported $CoSe_2$ nanoparticles in an acidic medium. Electrochim Acta 54:5252–5256
51. Sidik RA, Anderson AB (2006) Co_9S_8 as a catalyst for electroreduction of O_2: quantum chemistry predictions. J Phys Chem B 110:936–941
52. Toth L (1971) Transition metal carbides and nitrides, 1st edn. Academic Press, New York
53. Oyama ST (1996) The chemistry of transition metal carbides and nitrides. Springer, Dordrecht
54. Dong S, Chen X, Zhang X, Cui G (2013) Nanostructured transition metal nitrides for energy storage and fuel cells. Coord Chem Rev 257:1946–1956
55. Zellner MB, Chen JG (2005) Surface science and electrochemical studies of WC and W2C PVD films as potential electrocatalysts. Catal Today 99:299–307
56. Lee K, Ishihara A, Mitsushima S, Kamiya N, Ota K (2004) Stability and electrocatalytic activity for oxygen reduction in WC + Ta catalyst. Electrochim Acta 49:3479–3485
57. McIntyre DR, Vossen A, Wilde JR, Burstein GT (2002) Electrocatalytic properties of a nickel–tantalum–carbon alloy in an acidic electrolyte. J Power Sources 108:1–7
58. Hu Y, Jensen JO, Zhang W, Cleemann LN, Xing W, Bjerrum NJ, Li Q (2014) Hollow spheres of iron carbide nanoparticles encased in graphitic layers as oxygen reduction catalysts. Angew Chem Int Ed Engl 53:3749–3749
59. Jiang Y, Lu Y, Lv X, Han D, Zhang Q, Niu L, Chen W (2013) Enhanced catalytic performance of Pt-free iron phthalocyanine by graphene support for efficient oxygen reduction reaction. ACS Catal 3:1263–1271
60. Liang J, Zhou RF, Chen XM, Tang YH, Qiao SZ (2014) Fe-N decorated hybrids of CNTs grown on hierarchically porous carbon for high-performance oxygen reduction. Adv Mater 26:6074–6079
61. Zhou D, Yang L, Yu L, Kong J, Yao X, Liu W, Xu Z, Lu X (2015) Fe/N/C hollow nanospheres by Fe(III)-dopamine complexation-assisted one-pot doping as nonprecious-metal electrocatalysts for oxygen reduction. Nanoscale 7:1501–1509
62. Liu L, Yang X, Ma N, Liu H, Xia Y, Chen C, Yang D, Yao X (2016) Scalable and cost-effective synthesis of highly efficient Fe 2 N-based oxygen reduction catalyst derived from seaweed biomass. Small 12:1295–1301
63. Cao B, Neuefeind JC, Adzic RR, Khalifah PG (2015) Molybdenum nitrides as oxygen reduction reaction catalysts: structural and electrochemical studies. Inorg Chem 54:2128–2136
64. Sun T, Jiang Y, Wu Q, Du L, Zhang Z, Yang L, Wang X, Hu Z (2017) Is iron nitride or carbide highly active for oxygen reduction reaction in acidic medium? Cat Sci Technol 7:51–55
65. Smith AJ, Welch AJE (1960) Some mixed metal oxides of perovskite structure. Acta Crystallogr 13:653–656
66. Risch M (2017) Perovskite electrocatalysts for the oxygen reduction reaction in alkaline media. Catalysts 7:154
67. Zhu Y, Zhou W, Yu J, Chen Y, Liu M, Shao Z (2016) Enhancing electrocatalytic activity of perovskite oxides by tuning cation deficiency for oxygen reduction and evolution reactions. Chem Mater 28:1691–1697
68. Goldschmidt VM (1926) Die Gesetze der Krystallochemie. Naturwissenschaften 14:477–485
69. Ramadass N (1978) ABO3-type oxides—their structure and properties—a bird's eye view. Mater Sci Eng 36:231–239
70. Sunarso J, Torriero AAJ, Zhou W, Howlett PC, Forsyth M (2012) Oxygen reduction reaction activity of La-based perovskite oxides in alkaline medium: a thin-film rotating ring-disk electrode study. J Phys Chem C 116:5827–5834

71. Celorrio V, Dann E, Calvillo L, Morgan DJ, Hall SR, Fermin DJ (2016) Oxygen reduction at carbon-supported lanthanides: therole of the B-site. ChemElectroChem 3:283–291
72. Suntivich J, Gasteiger HA, Yabuuchi N, Nakanishi H, Goodenough JB, Shao-Horn Y (2011) Design principles for oxygen-reduction activity on perovskite oxide catalysts for fuel cells and metal-air batteries. Nat Chem 3:546–550
73. Larsson R, Johansson LY (1990) On the catalytic properties of mixed oxides for the electrochemical reduction of oxygen. J Power Sources 32:253–260
74. Hyodo T, Hayashi M, Miura N, Yamazoe N (1996) Catalytic activities of rare-earth manganites for cathodic reduction of oxygen in alkaline solution. J Electrochem Soc 143:L266–L267
75. Yuan X-Z, Li X, Qu W, Ivey DG, Wang H (2011) Electrocatalytic activity of non-stoichiometric perovskites toward oxygen reduction reaction in alkaline electrolytes. ECS Trans 35:11–20
76. Celorrio V, Calvillo L, Dann E, Granozzi G, Aguadero A, Kramer D, Russell AE, Fermín DJ (2016) Oxygen reduction reaction at $La_xCa_{1-x}MnO_3$ nanostructures: interplay between A-site segregation and B-site valency. Cat Sci Technol 6:7231–7238
77. Stoerzinger KA, Lü W, Li C, Ariando VT, Shao-Horn Y (2015) Highly active epitaxial $La_{(1-x)}Sr_xMnO_3$ surfaces for the oxygen reduction reaction: role of charge transfer. J Phys Chem Lett 6:1435–1440
78. Tulloch J, Donne SW (2009) Activity of perovskite $La_{1-x}Sr_xMnO_3$ catalysts towards oxygen reduction in alkaline electrolytes. J Power Sources 188:359–366
79. Hyodo T, Hayashi M, Mitsutake S, Miura N, Yamazoe N (1997) Praseodymium-calcium manganites ($Pr_{1-x}Ca_xMnO_3$) as electrode catalyst for oxygen reduction in alkaline solution. J Appl Electrochem 27:745–746
80. Takeda Y, Kanno R, Kondo T, Yamamoto O, Taguchi H, Shimada M, Koizumi M (1982) Properties of $SrMO_{3-\delta}$ (M=Fe, Co) as oxygen electrodes in alkaline solution. J Appl Electrochem 12:275–280
81. Du J, Zhang T, Cheng F, Chu W, Wu Z, Chen J (2014) Nonstoichiometric perovskite $CaMnO_{3-\delta}$ for oxygen electrocatalysis with high activity. Inorg Chem 53:9106–9114
82. Poux T, Bonnefont A, Kéranguéven G, Tsirlina GA, Savinova ER (2014) Electrocatalytic oxygen reduction reaction on perovskite oxides: series versus direct pathway. ChemPhysChem 15:2108–2120
83. Wei C, Feng Z, Scherer GG, Barber J, Shao-Horn Y, Xu ZJ (2017) Cations in octahedral sites: a descriptor for oxygen electrocatalysis on transition-metal spinels. Adv Mater 29:1–8
84. Verwey EJW, Heilmann EL (1947) Physical properties and cation arrangement of oxides with spinel structures I. Cation Arrangement in Spinels. J Chem Phys 15:174–180
85. Chakrapani K, Bendt G, Hajiyani H, Lunkenbein T, Greiner MT, Masliuk L, Salamon S, Landers J, Schlögl R, Wende H, Pentcheva R, Schulz S, Behrens M (2018) The role of composition of uniform and highly dispersed cobalt vanadium iron spinel nanocrystals for oxygen electrocatalysis. ACS Catal 8:1259–1267
86. Zhou Y, Xi S, Wang J, Sun S, Wei C, Feng Z, Du Y, Xu ZJ (2018) Revealing the dominant chemistry for oxygen reduction reaction on small oxide nanoparticles. ACS Catal 8:673–677
87. Zhao Q, Yan Z, Chen C, Chen J (2017) Spinels: controlled preparation, oxygen reduction/evolution reaction application, and beyond. Chem Rev 117:10121–10211
88. Chen D, Chen C, Baiyee ZM, Shao Z, Ciucci F (2015) Nonstoichiometric oxides as low-cost and highly-efficient oxygen reduction/evolution catalysts for low-temperature electrochemical devices. Chem Rev 115:9869–9921
89. Si C, Zhang Y, Zhang C, Gao H, Ma W, Lv L, Zhang Z (2017) Mesoporous nanostructured spinel-type MFe_2O_4 (M = Co, Mn, Ni) oxides as efficient bi-functional electrocatalysts towards oxygen reduction and oxygen evolution. Electrochim Acta 245:829–838
90. Hong W, Li L, Xue R, Xu X, Wang H, Zhou J, Zhao H, Song Y, Liu Y, Gao J (2017) One-pot hydrothermal synthesis of Zinc ferrite/reduced graphene oxide as an efficient electrocatalyst for oxygen reduction reaction. J Colloid Interface Sci 485:175–182

91. Zhu H, Zhang S, Huang Y-X, Wu L, Sun S (2013) Monodisperse $M_xFe_{3-x}O_4$ (M = Fe, Cu, Co, Mn) nanoparticles and their electrocatalysis for oxygen reduction reaction. Nano Lett 13:2947–2951
92. Bhandary N, Ingole PP, Basu S (2018) Electrosynthesis of Mn-Fe oxide nanopetals on carbon paper as bi-functional electrocatalyst for oxygen reduction and oxygen evolution reaction. Int J Hydrog Energy 43:3165–3171
93. Gong K, Du F, Xia Z, Durstock M, Dai L (2009) Nitrogen-doped carbon nanotube arrays with high electrocatalytic activity for oxygen reduction. Science 323:760–764
94. Liu M, Zhang R, Chen W (2014) Graphene-supported nanoelectrocatalysts for fuel cells: synthesis, properties, and applications. Chem Rev 114:5117–5160
95. Lin Z, Waller GH, Liu Y, Liu M, Wong C (2013) 3D nitrogen-doped graphene prepared by pyrolysis of graphene oxide with polypyrrole for electrocatalysis of oxygen reduction reaction. Nano Energy 2:241–248
96. Wang H, Maiyalagan T, Wang X (2012) Review on recent progress in nitrogen-doped graphene: synthesis, characterization, and its potential applications. ACS Catal 2:781–794
97. Liang Y, Wang H, Diao P, Chang W, Hong G, Li Y, Gong M, Xie L, Zhou J, Wang J, Regier TZ, Wei F, Dai H (2012) Oxygen reduction electrocatalyst based on strongly coupled cobalt oxide nanocrystals and carbon nanotubes. J Am Chem Soc 134:15849–15857
98. Nie R, Bo X, Luhana C, Nsabimana A, Guo L (2014) Simultaneous formation of nitrogen and sulfur-doped carbon nanotubes-mesoporous carbon and its electrocatalytic activity for oxygen reduction reaction. Int J Hydrog Energy 39:12597–12603
99. Liang J, Jiao Y, Jaroniec M, Qiao SZ (2012) Sulfur and nitrogen dual-doped mesoporous graphene electrocatalyst for oxygen reduction with synergistically enhanced performance. Angew Chem Int Ed Engl 124:11664–11668
100. Nasini UB, Gopal Bairi V, Kumar Ramasahayam S, Bourdo SE, Viswanathan T, Shaikh AU (2014) Oxygen reduction reaction studies of phosphorus and nitrogen co-doped mesoporous carbon synthesized via microwave technique. ChemElectroChem 1:573–579
101. Choi CH, Chung MW, Park SH, Woo SI (2013) Additional doping of phosphorus and/or sulfur into nitrogen-doped carbon for efficient oxygen reduction reaction in acidic media. Phys Chem Chem Phys 15:1802–1805
102. Wang S, Zhang L, Xia Z, Roy A, Chang DW, Baek J-B, Dai L (2012) BCN graphene as efficient metal-free electrocatalyst for the oxygen reduction reaction. Angew Chem Int Ed Engl 51:4209–4212
103. Shao Y, Zhang S, Engelhard MH, Li G, Shao G, Wang Y, Liu J, Aksay IA, Lin Y (2010) Nitrogen-doped graphene and its electrochemical applications. J Mater Chem 20:7491
104. Geng D, Chen Y, Chen Y, Li Y, Li R, Sun X, Ye S, Knights S (2011) High oxygen-reduction activity and durability of nitrogen-doped graphene. Energy Environ Sci 4:760
105. Carrillo-Rodríguez JC, Alonso-Lemus IL, Siller-Ceniceros AA, Martínez GE, Pizá-Ruiz P, Vargas-Gutiérrez G, Rodríguez-Varela FJ (2017) Easy synthesis of N-doped graphene by milling exfoliation with electrocatalytic activity towards the Oxygen Reduction Reaction (ORR). Int J Hydrog Energy 42:30383–30388
106. Alonso-Lemus IL, Figueroa-Torres MZ, García-Hernández AB, Escobar-Morales B, Rodríguez-Varela FJ, Fuentes AF, Lardizabal-Gutierrez D, Quintana-Owen P (2017) Low-cost sonochemical synthesis of nitrogen-doped graphene metal-free electrocatalyst for the oxygen reduction reaction in alkaline media. Int J Hydrog Energy 42(21):30330–30338
107. Pels JR, Kapteijn F, Moulijn JA, Zhu Q, Thomas KM (1995) Evolution of nitrogen functionalities in carbonaceous materials during pyrolysis. Carbon 33:1641–1653
108. Yan L, Yu J, Houston J, Flores N, Luo H (2017) Biomass derived porous nitrogen doped carbon for electrochemical devices. Green Energy Environ 2:84–99
109. Yang S, Zhao G-L, Khosravi E (2010) First principles studies of nitrogen doped carbon nanotubes for dioxygen reduction. J Phys Chem C 114:3371–3375
110. Reda M, Hansen HA, Vegge T (2018) DFT study of stabilization effects on N-doped graphene for ORR catalysis. Catal Today 312:118–125

111. Zhang L, Xia Z (2011) Mechanisms of oxygen reduction reaction on nitrogen-doped graphene for fuel cells. J Phys Chem C 115:11170–11176
112. Yu H, Shang L, Bian T, Shi R, Waterhouse GIN, Zhao Y, Zhou C, Wu L-Z, Tung C-H, Zhang T (2016) Nitrogen-doped porous carbon nanosheets templated from g-C3N4 as metal-free electrocatalysts for efficient oxygen reduction reaction. Adv Mater 28:5080–5086
113. He C, Li Z, Cai M, Cai M, Wang J-Q, Tian Z, Zhang X, Shen PK (2013) A strategy for mass production of self-assembled nitrogen-doped graphene as catalytic materials. J Mater Chem A 1:1401–1406
114. Luo Z, Lim S, Tian Z, Shang J, Lai L, MacDonald B, Fu C, Shen Z, Yu T, Lin J (2011) Pyridinic N doped graphene: synthesis, electronic structure, and electrocatalytic property. J Mater Chem 21:8038
115. Feng L, Chen Y, Chen L (2011) Easy-to-operate and low-temperature synthesis of gram-scale nitrogen-doped graphene and its application as cathode catalyst in microbial fuel cells. ACS Nano 5:9611–9618
116. Deng D, Pan X, Yu L, Cui Y, Jiang Y, Qi J, Li W-X, Fu Q, Ma X, Xue Q, Sun G, Bao X (2011) Toward N-doped graphene via solvothermal synthesis. Chem Mater 23:1188–1193
117. Tavakol H, Keshavarzipour F (2016) A sulfur doped carbon nanotube as a potential catalyst for the oxygen reduction reaction. RSC Adv 6:63084–63090
118. Zhang L, Niu J, Li M, Xia Z (2014) Catalytic mechanisms of sulfur-doped graphene as efficient oxygen reduction reaction catalysts for fuel cells. J Phys Chem C 118:3545–3553
119. Seredych M, László K, Bandosz TJ (2015) Sulfur-doped carbon aerogel as a metal-free oxygen reduction catalyst. ChemCatChem 7:2924–2931
120. Wang L, Dong H, Guo Z, Zhang L, Hou T, Li Y (2016) Potential application of novel boron-doped graphene nanoribbon as oxygen reduction reaction catalyst. J Phys Chem C 120:17427–17434
121. Su J, Cao X, Wu J, Jin C, Tian J-H, Yang R (2016) One-pot synthesis of boron-doped ordered mesoporous carbons as efficient electrocatalysts for the oxygen reduction reaction. RSC Adv 6:24728–24737
122. Lin Y, Zhu Y, Zhang B, Kim YA, Endo M, Su DS (2015) Boron-doped onion-like carbon with enriched substitutional boron: the relationship between electronic properties and catalytic performance. J Mater Chem A 3:21805–21814
123. Guo M, Huang J, Kong X, Peng H, Shui H, Qian F, Zhu L, Zhu W, Zhang Q (2016) Hydrothermal synthesis of porous phosphorus-doped carbon nanotubes and their use in the oxygen reduction reaction and lithium-sulfur batteries. New Carbon Mater 31:352–362
124. Zhang X, Lu Z, Fu Z, Tang Y, Ma D, Yang Z (2015) The mechanisms of oxygen reduction reaction on phosphorus doped graphene: a first-principles study. J Power Sources 276:222–229
125. Liu Z, Fu X, Li M, Wang F, Wang Q, Kang G, Peng F (2015) Novel silicon-doped, silicon and nitrogen-codoped carbon nanomaterials with high activity for the oxygen reduction reaction in alkaline medium. J Mater Chem A 3:3289–3293
126. Sun X, Zhang Y, Song P, Pan J, Zhuang L, Xu W, Xing W (2013) Fluorine-doped carbon blacks: highly efficient metal-free electrocatalysts for oxygen reduction reaction. ACS Catal 3:1726–1729
127. Yao Z, Nie H, Yang Z, Zhou X, Liu Z, Huang S (2012) Catalyst-free synthesis of iodine-doped graphenevia a facile thermal annealing process and its use for electrocatalytic oxygen reduction in an alkaline medium. Chem Commun 48:1027–1029
128. Mena-Durán CJ, Alonso-Lemus IL, Quintana P, Barbosa R, Ordoñez LC, Escobar B (2018) Preparation of metal-free electrocatalysts from cassava residues for the oxygen reduction reaction: a sulfur functionalization approach. Int J Hydrog Energy 43:3172–3179
129. Yang S, Mao X, Cao Z, Yin Y, Wang Z, Shi M, Dong H (2018) Onion-derived N, S self-doped carbon materials as highly efficient metal-free electrocatalysts for the oxygen reduction reaction. Appl Surf Sci 427:626–634

130. Sun Y, Wu J, Tian J, Jin C, Yang R (2015) Sulfur-doped carbon spheres as efficient metal-free electrocatalysts for oxygen reduction reaction. Electrochim Acta 178:806–812
131. Yang Z, Yao Z, Li G, Fang G, Nie H, Liu Z, Zhou X, Chen X, Huang S (2012) Sulfur-doped graphene as an efficient metal-free cathode catalyst for oxygen reduction. ACS Nano 6:205–211
132. Inamdar S, Choi H-S, Wang P, Song MY, Yu J-S (2013) Sulfur-containing carbon by flame synthesis as efficient metal-free electrocatalyst for oxygen reduction reaction. Electrochem Commun 30:9–12
133. Sun X, Song P, Zhang Y, Liu C, Xu W, Xing W (2013) A class of high performance metal-free oxygen reduction electrocatalysts based on cheap carbon blacks. Sci Rep 3:2505
134. Li Y, Chopra N (2015) Progress in large-scale production of graphene. Part 2: vapor methods. JOM 67:44–52
135. Luque R (2013) Producing fuels and fine chemicals from biomass using nanomaterials, 1st edn. CRC Press, Boca Raton
136. Antolini E (2016) Nitrogen-doped carbons by sustainable N- and C-containing natural resources as nonprecious catalysts and catalyst supports for low temperature fuel cells. Renew Sust Energ Rev 58:34–51
137. Alonso-Lemus IL, Rodriguez-Varela FJ, Figueroa-Torres MZ, Sanchez-Castro ME, Hernandez-Ramírez A, Lardizabal-Gutierrez D, Quintana-Owen P (2016) Novel self-nitrogen-doped porous carbon from waste leather as highly active metal-free electrocatalyst for the ORR. Int J Hydrog Energy 41:23409–23416
138. Lardizabal-Guitierrez D, González-Quijano D, Bartolo-Pérez P, Escobar-Morales B, Rodríguez-Varela FJ, Alonso-Lemus IL (2016) Communication—synthesis of self-doped metal-free electrocatalysts from waste leather with high ORR activity. J Electrochem Soc 163:H15–H17
139. Zhang J, Wu S, Chen X, Pan M, Mu S (2014) Egg derived nitrogen-self-doped carbon/carbon nanotube hybrids as noble-metal-free catalysts for oxygen reduction. J Power Sources 271:522–529
140. Liu F, Peng H, Qiao X, Fu Z, Huang P, Liao S (2014) High-performance doped carbon electrocatalyst derived from soybean biomass and promoted by zinc chloride. Int J Hydrog Energy 39:10128–10134
141. Gao S, Geng K, Liu H, Wei X, Zhang M, Wang P, Wang J (2015) Transforming organic-rich amaranthus waste into nitrogen-doped carbon with superior performance of the oxygen reduction reaction. Energy Environ Sci 8:221–229
142. Zhai Y, Zhu C, Wang E, Dong S (2014) Energetic carbon-based hybrids: green and facile synthesis from soy milk and extraordinary electrocatalytic activity towards ORR. Nanoscale 6:2964
143. Lu J, Bo X, Wang H, Guo L (2013) Nitrogen-doped ordered mesoporous carbons synthesized from honey as metal-free catalyst for oxygen reduction reaction. Electrochim Acta 108:10–16
144. Pan F, Cao Z, Zhao Q, Liang H, Zhang J (2014) Nitrogen-doped porous carbon nanosheets made from biomass as highly active electrocatalyst for oxygen reduction reaction. J Power Sources 272:8–15
145. Li J, Wang S, Ren Y, Ren Z, Qiu Y, Yu J (2014) Nitrogen-doped activated carbon with micrometer-scale channels derived from luffa sponge fibers as electrocatalysts for oxygen reduction reaction with high stability in acidic media. Electrochim Acta 149:56–64
146. Escobar B, Pérez-Salcedo KY, Alonso-Lemus IL, Pacheco D, Barbosa R (2017) N-doped porous carbon from Sargassum spp. as metal-free electrocatalysts for oxygen reduction reaction in alkaline media. Int J Hydrog Energy 42(51):30274–30283
147. Song MY, Park HY, Yang D-S, Bhattacharjya D, Yu J-S (2014) Seaweed-derived heteroatom-doped highly porous carbon as an electrocatalyst for the oxygen reduction reaction. ChemSusChem 7:1755–1763
148. Chaudhari KN, Song MY, Yu JS (2014) Transforming hair into heteroatom-doped carbon with high surface area. Small 10:2625–2636

149. Chaudhari NK, Song MY, Yu J-S (2015) Heteroatom-doped highly porous carbon from human urine. Sci Rep 4:5221
150. Wang R, Wang K, Wang Z, Song H, Wang H, Ji S (2015) Pig bones derived N-doped carbon with multi-level pores as electrocatalyst for oxygen reduction. J Power Sources 297:295–301
151. Guo C-Z, Chen C-G, Luo Z-L (2014) A novel nitrogen-containing electrocatalyst for oxygen reduction reaction from blood protein pyrolysis. J Power Sources 245:841–845